# Research on the Initiation of Multiple Upward Leaders From a Single Structure Based on an Improved Lightning Attachment Model

**Yuhe Lin[1,2], Yongbo Tan[1], Junhao Yu[1], Qi Qi[2], Bin Wu[2], Weitao Lyu[2]**

[1]Key Laboratory of Meteorological Disaster, Ministry of Education, Joint International Research Laboratory of Climate and Environment Change, Collaborative Innovation Center on Forecast and Evaluation of Meteorological Disasters, Key Laboratory for Aerosol-Cloud-Precipitation of China Meteorological Administration, Nanjing University of Information Science and Technology, Nanjing, China.

[2]State Key Laboratory of Severe Weather, Chinese Academy of Meteorological Sciences, Beijing, China.

Corresponding author: Yongbo Tan(ybtan@ustc.edu)
Weitao Lyu(lyuwt@foxmail.com)

**Key Points:**

- An improved 3-D fine-resolution stochastic discharge model is established
- Reasons for the inception of multiple upward leaders instead of a single upward leader are discussed

## Abstract

More and more optical records have exhibited that multiple upward leaders (MULs) occur frequently on a structure in the flash attachment process. An interesting issue is why a structure can continue to launch upward leader (UL) after the first one appears. This phenomenon is analyzed in the present paper. Considering the influence of the leader behaviors on the ambient electric field, an improved 3-D fine-resolution lightning attachment model with MULs is established to simulate cloud-to-ground flash events with diverse leader spatial morphologies. The simulation results show that MULs may initiate almost simultaneously or with an obvious delay and the variation range of UL length is large. From this, the flash events of lightning terminating on a structure are divided into four scenarios and each scenario is analyzed. It can be found that the spatial location of downward leader, the length and propagation direction of the first UL and the time interval from the inception of the first UL to final jump significantly affect the electric fields at top corners of structure and further affect the inception of the second UL. Based on qualitative analysis, four factors are proposed to explain why the above four scenarios happen.


## 1 Introduction

The physical mechanism of Could-to-ground (CG) lightning attachment to grounded structures is one of the most important issues in lightning physics research. It is generally assumed that the attachment process includes the inception and propagation of one upward leader (UL) or multiple upward leaders (MULs) and the final jump (Rakov & Uman, 2003; Tran & Rakov, 2017). As the downward leader (DL) approaches, the first upward leader (FUL) initiates from the structure when certain conditions are met. After that, FUL and DL continue to propagate tortuously, showing a variety of spatial morphologies. The second upward leader (SUL) can sometimes initiate from the same building but not always (e.g., Lu et al., 2012; Qi et al., 2021; Saba et al., 2017).

Thanks to recent observation research, more details of leader propagation and

connection have been captured, which is useful to improve our understanding of the attachment process (Lu et al., 2013; Stolzenburg et al., 2015; Tran et al., 2014; Wang et al., 2019). Besides, a number of photos and video recordings have proved the MULs occur frequently in CG lightning attachment process, which may initiate from the different structures or the same one (e.g., Lu et al., 2012; Qi et al., 2021; Saba et al., 2017). So why does a building sometimes launch MULs but sometimes only one UL? Regrettably, previous studies have yet to answer this question. Due to optical instrumentation is hard to identify the UL with shorter length and lower luminosity, the UL must develop to a visible length to be captured, which results in few images documenting the moment when the UL is triggered. Therefore, it is laborious to answer the above question only through optical data.

Based on the observational facts, various models have been established to study the electrification and discharge process. At present, there are two main types of lightning leader models for simulation of the attachment process, the physical model and the stochastic model. Several scholars used physical models which take into account complex factors, such as induced charge and corona region, to analyze the micro-physical process of UL inception (e.g., Aleksandrov et al., 2001; Bazelyan et al., 2009; Becerra & Cooray, 2006). As confirmed by researchers, the inception of FUL goes through a sequence of processes including glow corona, streamer, and streamer-to-leader transition. Such models can reproduce the microscopic process of initial discharge in detail, while the DLs simulated by most physical models are branches and the UL always extends toward to DL without bending. In reality, DL and FUL always exhibit complex spatial morphologies (e.g., Lu et al., 2012; Qi et al., 2019). Zhou et al. (2021) studied the effects of the UL on electromagnetic fields for lightning striking to tall towers. And Cooray et al. (2010) presented the effect of the competition between multiple leaders. Given this, we believe the leader behaviors in attachment process should not be ignored because it is one of the important factors affecting the SUL inception.

The stochastic model which was extended from the dielectric breakdown model by Mansell et al. (2002) and later improved by many researchers (e.g., Iudin et al., 2017; Tan et al., 2006), has been widely used to investigate the intracloud lightning (e.g., Riousset et al., 2007; Tao et al., 2009). In recent years, an improved stochastic model for CG flash has been presented by Jiang et al. (2020) to analyze the distribution of lightning strike points influenced by tall structures. The stochastic model simulates only the macroscopic properties of discharge channels and does not deal with the microscopic processes of breakdown. While a significant advantage of stochastic model is that it is capable of producing branched DL channel and tortuous nature of leaders (Mansell et al., 2002). For this reason, most scholars who applied stochastic models were focusing more on leader behaviors or lightning structures (Iudin et al., 2017; Syssoev et al., 2020; Xu et al., 2021), and this is an important reason why the stochastic model is chosen to research the inception of SUL in this paper. Limited by the simulation efficiency, existing stochastic models can hardly satisfy both 3-D and fine-resolution simulation needs. But we all know that the 3-D models can produce more realistic lightning discharges to a certain degree and space resolution is an important factor affecting the simulation accuracy of the tip electric field at grounded structures (Tan et al., 2014a). Both of them affect the simulation results of the CG flashes. Therefore, improving the space resolution as much as possible in a larger 3-D simulated domain is an important trend in model development.

This paper is interested in whether a SUL can initiate from the same structure after the FUL occurs. Considering the impact of leader behaviors on the ambient electric field, an improved 3-D fine-resolution CG lightning attachment model with MULs is established. We utilize this model to simulate the development and attachment process of leaders under the influence of a single structure and find relevant factors to explain the reasons for the inception of one or more ULs from a structure.

## 2 Model description

The GPU parallel computing technology which shows the surprising capability to

speed up iterative tasks makes the 3-D fine-resolution simulation in a larger domain possible. Using CPU serial algorithm and GPU parallel algorithm, an improved 3-D fine-resolution Lightning Attachment Model with MULs (LAMM) is established based on the stochastic discharge parameterization scheme (Dul'zon et al., 1999; Jiang et al., 2020; Mansell et al., 2002; Tan et al., 2014b). LAMM is suitable for studying the influence of leader/lightning spatial morphology or the impact of grounded-objects on discharge in the near-ground domain during the attachment process. The domain size and space resolution in LAMM can be adjusted freely according to requirements of research, taking into account running time and memory limit. As shown in Figure 1, one or more structures with any sizes are allowed to be placed anywhere on the ground, and each of them may initiate one or more upward leaders. The detailed introduction of LAMM is as follows:

## 2.1 The propagation of DL

LAMM simulates the negative CG flashes which are most common in flash events (Rakov & Uman, 2003). Considering this article is dedicated to studying the UL inception in the lightning attachment process, the LAMM does not simulate the discharge process in the thunderstorm, but sets an initial downward-moving leader whose length is 25m at a random location at the top of the simulation domain with an initial potential of -25MV, which is similar to the assumption in Jiang et al. (2020), Mazur et al. (2000).

The leader channel is treated as a conductor with internal electric field of 500V/m (Mansell et al., 2002; Tan et al., 2006). And LAMM simulates the macroscopic extension of DL as a step-by-step stochastic process (Jiang et al., 2020; Mansell et al., 2002; Tan et al., 2014b; Wang et al., 2016). In observations of lightning propagation, since Biagi et al. (2009) presented the first high-speed video images of space stems/leaders, more and more high-speed video cameras have captured many space stems/leaders around the DL channel during the development of DL (e.g., Biagi et al.,2014; Hill et al., 2011). Some of them connected to the leader channel and made

transition to the part of lightning, others made connection to DL briefly and then died off (Biagi et al., 2014; Qi, et al., 2016; Wang et al., 2019). Referring to the observations, we believe that the DL channel points will disappear if there are no new extensions connected to them for a long time. Therefore, after each new extension of DL, LAMM cuts off the channel points that have been stagnant from all existing channel points and their effect on the ambient electric field disappears as they pass off. After identifying all continuously channel points, the potential gradients between them and ambient grid points are recomputed. Since propagation threshold proposed by researchers is about 100-500kV/m (Mansell et al., 2002; Tan et al., 2006; Iudin et al., 2017), the next channel point is selected randomly from all possible new extensions for which the potential gradient is larger than the propagation threshold of 220kV/m. And the probability of choosing a new extension is given by the formulation in (Mansell et al., 2002).

In Figure 1, the DL channel points which died out during the discharge are shown in purple, and those that propagate continuously are shown in blue. Unfortunately, compared to the model developed by Syssoev et al. (2020) or by Iudin et al. (2017), LAMM can only crudely reproduce the decay of channel points from a macroscopic perspective, which is somewhat simplistic. But it can effectively prevent too many lighting branches from being generated and make structure immersed in a reasonable electric field produced by DL to a certain extent.

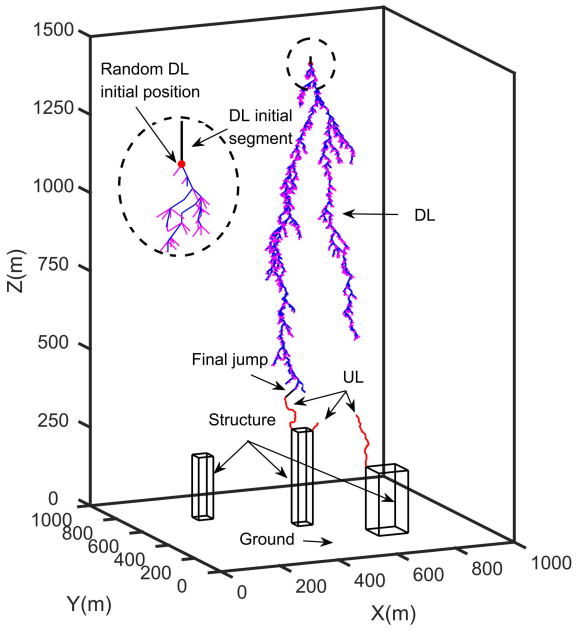

**Figure 1.** The 3-D plot of a CG lightning simulated by LAMM. The structures are represented by the black rectangles. The red dot at the top of domain denotes the random initial position of the DL. The vertical black segment at the top denotes the initial segment of the DL. DL channel points which died out during the discharge are shown in purple, and the lightning channel points that propagate continuously are shown in blue. The red lines denote ULs. The black segment at the end of the DL channel denotes the final jump. The legends of the following 3-D plots of CG flashes are the same as this figure legend and show the eventually DL channel existing in the domain.

## 2.2 Initiation and propagation of MULs

Although the LAMM does not include cloud model, it retains the background electric field produced by the thundercloud to a certain extent. The same as Jiang et al. (2020), the background electric field strength at the ground and the top boundary is set at -5kV/m and -90kV/m, respectively, with the increasing trend among them by referring to the previous measurements of the electric field underneath a thundercloud at particular heights (Biagi et al., 2011; Chauzy et al., 1991). Consistent with optical photos (Lu et al., 2012; Qi et al., 2019), LAMM allows MULs to initiate simultaneously or with a delay from different structures or the same one. The leader initiation threshold is generally considered to be around 200-500kV/m (Becerra et al., 2008; Gurevich & Zybin, 2001; Mazur et al., 2000; Petrov et al., 2003). Therefore, after updating electric potential at each grid point in time, the LAMM searches the grid points on the structure surface and the ground that meet the UL initiation threshold of 250kV/m. And the new extension of UL is chosen randomly from the grid points above the tip of the existing UL channel, with the probability for choosing a particular direction depending on the potential gradient. Since most images recorded the UL without obvious branches in the near ground region (e.g., Krider & Ladd, 1975; Saba et al., 2017; Warner, 2010), the new extension of UL can only extend from the existing UL tip. Like the DL extension, the electric fields at all grid points in the domain need to be recalculated after each extension of UL. In this way, the tortuous

development of one or more ULs with diverse leader behaviors can be produced. It is worth noting that the step-by-step stochastic scheme is applied to the propagation process each leader (including DL and each UL) independently, that is, the positive and negative leaders may extend simultaneously and MULs propagate at the same time.

### 2.3 The speed ratio and connection of DL and UL

In general, the average velocity of DL is greater than the velocity of UL in the same CG lightning (e.g., Saba et al., 2017; Yokoyama et al., 1990). Since no timescale is assumed for the discharge development in LAMM, the speed of positive and negative leaders similar to observational records cannot be calculated. However, previous studies (e.g., Arevalo & Cooray, 2009; Becerra & Cooray, 2008; Petrov & D'Alessandro, 2002) have confirmed the leader speed affects the development of leaders and thus the attachment process. For this reason, even if the speed cannot be reproduced well, it cannot be omitted. Laboratory experiments on long rod-rod air gaps show that the ratio of the initial velocity of a positive upward leader to that of a negative downward leader is about 1 : 4 (Chernov et al., 1991; Petrov et al., 1994). And Saba et al. (2017) recorded the speed ratio of 2.3, 3.1, and 4.8 from three CG flash events. From that, we set the speed ratio of DL to UL is 4:1 (Jiang et al., 2020; Petrov & D'Alessandro, 2002), that is, when DL propagates four steps, UL propagates one step. The sequence in which channel segments (steps) are added can be considered a kind of time ordering, and it is used to indirectly reflect time in this paper. In addition, to simulate two basic leader connection scenarios (‘tip-to-tip’ and ‘DL’s tip to UL’s lateral surface’) observed by (Lu et al., 2013, 2016), the potential gradient between the DL tip and each channel point of UL is calculated after each new extension. If the attachment threshold of 500kV/m is met (Becerra & Cooray, 2008; Dellera & Garbagnati, 1990; Jiang et al., 2020), the DL tip is connected to the UL channel.

### 2.4 Method of improving computational efficiency

In LAMM, the continuous-space is discretized into numerous grid points. The ground, structures, leader channel, and upper boundary of the simulation domain are defined to satisfy the Dirichlet boundary condition. The side boundary of the simulation domain satisfies the Neumann boundary condition. Calculating electric field in all directions for each grid point, that is, solving Poisson's equation with particular boundary conditions, is the most time-consuming portion of the simulation process. However, simulating a 3-D fine-resolution CG flash attachment process in a larger domain means it has to calculate the electric fields of tens of millions of grid points. If only using traditional CPU serial algorithm, the computational efficiency is very low.

To solve this problem, our model adopts GPU parallel computing, which enables to perform several tasks at once instead of one-by-one like a CPU needs to, to accelerate electric field calculation. In order to run smoothly on the GPU, a slight modification is made to remove the data dependency in the iterative process. However, in the lightning numerical model, except the code portions related to electric field calculation, there is massive code involving loops etc. Such code is executed on the CPU, because it slows down the GPU. Combining CPU serial algorithm and GPU parallel algorithm significantly boosts the computational efficiency of numerical simulation. In LAMM, this method is used as follows: After each new extension of leader, the electric fields at all grid points in domain are recalculated on the GPU and then the updated electric field data are transferred to the CPU for further processing. Repeat this process to extend the leader channel.

## 3 Simulation Results

To discuss the effect of leader's spatial behaviors on UL initiation, 300 CG flash simulations are performed by using LAMM. The simulation domain is 1000m × 1000m × 1500m, which is discretized using 5m × 5m × 5m equidistant grids. A 300m-height structure with a length and width of 50m is placed in the middle of ground. The simulation results of four CG lightnings are shown in Figure 2.

DL, initiating from a random position at 1500m height, may propagate downward in any direction. The simulated lightning channels exhibit diverse spatial morphologies, such as DL with only one main channel (Figures 2a and 2b) or DL with multiple noticeable branches (Figures 2c and 2d). Both main channel and branches zigzag toward the ground, which resemble actual CG flashes (e.g., Lu et al., 2012; Qi et al., 2019; Tran et al., 2014). As DL approaches, the structure may launch one UL (Figures 2c and 2d) or MULs (Figures 2a and 2b). And most ULs initiate from top corners of the structure due to electric field intensification by the tips of structure (Bermudez et al., 2001; Motoyama et al., 1996; Tan et al., 2014a). In a few cases, the lightning strikes the side of structure or ground, such events are not discussed in this paper. Once UL occurs, it zigzag upwards without bifurcation. Although the overall UL channel tends to be toward the DL because of the attraction between positive and negative leaders, the propagation direction of UL may change several times in a flash event (Figures 2b, 2c and 2d), which is similar to the development of leaders recorded by cameras (Qi et al., 2019; Saba et al., 2017; Warner, 2010). When the final jump condition is reached, LAMM can reproduce two basic leader connection scenarios documented in the optical data, namely, the tip of DL to the tip of upward connecting leader (Figures 2a, 2c and 2d) and the DL's tip to the lateral surface of UL (Figure 2b) (Lu et al., 2013, 2016). From the simulation results, we believe that LAMM is reasonable and has advantages in studying the leader behaviors during the attachment process because it can simulate a wide various structures of leaders and successfully reproduce the tortuous development of leaders.

This paper focuses on whether the SUL can be triggered after FUL occurs. Therefore, only the flash events with one or two ULs are considered (The MULs mentioned later represent two ULs). We analyzed all CG lightning events with MULs, and found the length of FUL and SUL may be similar or significantly different in a concrete event, which depends on whether positive leaders initiate almost simultaneously or with an obvious delay. For example, in Figure 2a, SUL initiates after FUL extends 4 steps, while in Figure 2b the SUL does not occur until FUL propagates 68 steps. Similar

lightning events have been observed by several investigators (Lu et al., 2012; Qi et al., 2019). For an in-depth study, the simulated results of DL terminating on a structure are divided into the following four scenarios: A, FUL and SUL with similar lengths initiate almost simultaneously (Figure 2a); B, SUL is triggered much later than FUL, causing the length of MULs to be quite different (Figure 2b); C, a single UL with short length occurs on structure (Figure 2c); D, the structure launches only one long-length UL (Figure 2d). Note that if the length of UL is more than 300m, which is the height of the structure, we consider a long-length UL is generated. The number of samples for each situation is shown in Table 1.

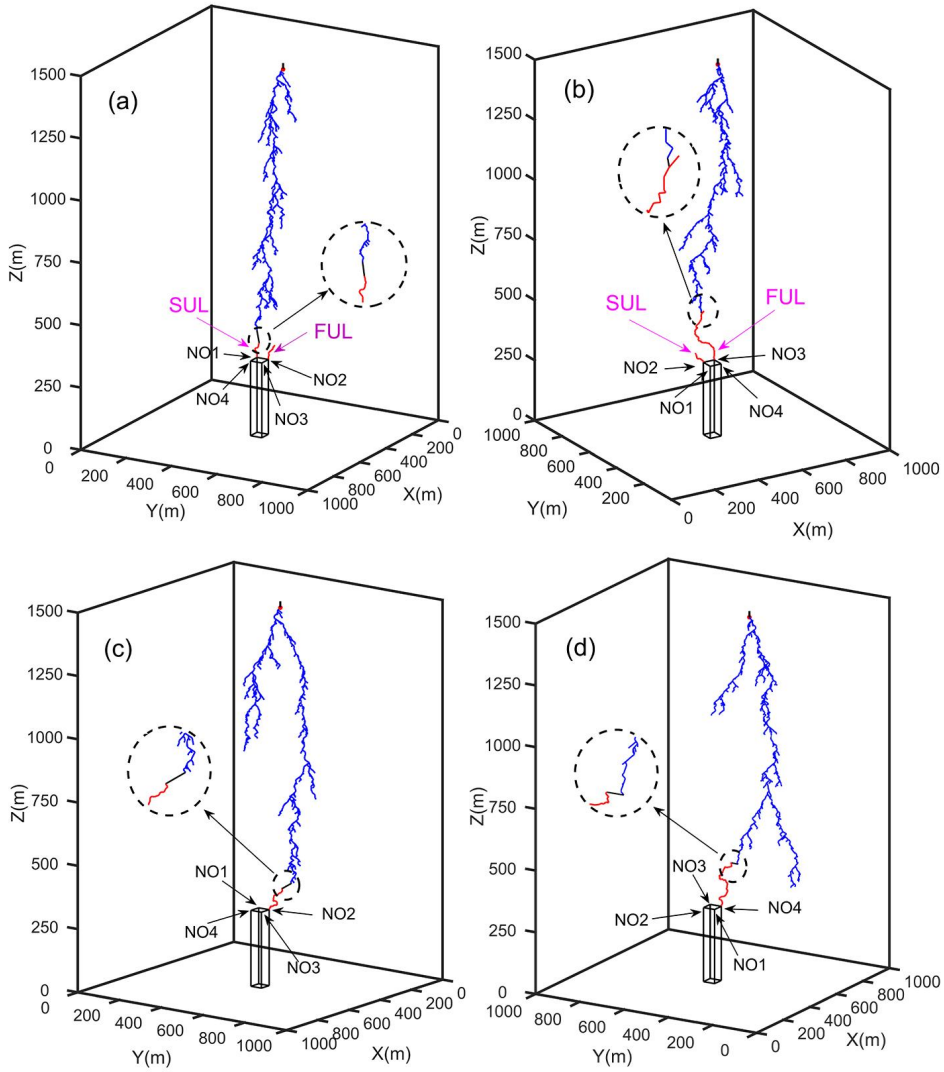


**Figure 2.** Simulation Results: (a) A case of scenario A, FUL from corner NO2 and SUL from corner NO1 almost initiate simultaneously. The flash attachment process exhibits the connection of the DL's tip to the UL's tip. (b) A case of scenario B, SUL

appearing on corner NO2 is triggered much later than the FUL appearing on corner NO3. The flash attachment process exhibits the connection of the DL's tip to the lateral surface of UL. (c) A case of scenario C, a single short-length UL is triggered. A flash strikes the structure with a tip-to-tip attachment. (d) A case of scenario D, a single long-length UL is triggered. A flash strikes the structure with a tip-to-tip attachment. In this paper, a UL whose length is more than 300m is considered a long-length UL. NO1~NO4 are the four top corners of the structure with spatial coordinates (475,475,1500)、(475,525,1500)、(525,525,1500)、(525,475,1500). In each 3-D plot, the viewing angle is adjusted to better show the simulation results. The details are the same as in Figure 1.

**Table 1.** Number of Samples for Each Situation in 300 CG Flash Simulations

| Total | Lightning strikes the structure | | | | | Lightning strikes the ground |
|---|---|---|---|---|---|---|
| | Two ULs | | Only one UL | | More than two ULs | |
| | Scenario A | Scenario B | Scenario C | Scenario D | | |
| 300 | 48 | 75 | 65 | 41 | 9 | 62 |

## 4 Discussion

Recently, more and more published lightning photographs show MULs emanating from a single structure (e.g., Lu et al., 2012; Qi et al., 2021; Saba et al., 2017). Although the inception of MULs is caused by many factors, a general consensus is that the electric field that meets particular conditions is a prerequisite for UL initiation. Based on physical models, scientists determined the electric field by simulating the microscopic discharge process, involving factors such as the space charges and corona region (Aleksandrov et al., 2001; Bazelyan et al., 2009; Becerra & Cooray, 2006). Compared with physical models, LAMM simplifies the microscopic processes of breakdown. While it can simulate the macroscopic properties of discharge channels and well exhibit the influence of leader spatial morphology on electric field, which is this paper focus on. We admit that LAMM is somewhat simplistic to obtain the initiation threshold, but it is not a fatal flaw for our research purpose. The following sections discuss the inception of MULs.

300 4.1 A case study

301 An example of scenario B is analyzed as follows. Figure 3a depicts the development
302 of leaders in 3D simulated domain and its 2D projection onto the x-y plane. From
303 Figure 3a, it can be seen that the DL channel is irregular and its spatial location is
304 asymmetrical with respect to the structure. As DL propagates, FUL appears on corner
305 NO2 and then extends zigzag upward. Due to the tortuous development of FUL, it
306 behaves differently for different top corners. For corners NO3 and NO4, it continues
307 to extend away from them. While for the corner NO1 where SUL occurs, FUL first
308 extends away until FUL tip is 82.5m horizontally from it and then bents toward to
309 corner NO1 until FUL tip is 51.5m horizontally from it, after that, FUL propagates
310 away from corner NO1 again (see Figure 3a). In this case, the total length of the FUL
311 is 527.5m, which is within length values of upward connecting leaders range from
312 180 to 818m observed by Gao et al. (2014). When the FUL length is 442.5m, SUL
313 initiates from corner NO1.

314 During the development of leaders, the electric field changes at four top corners of
315 structure as shown in Figure 3b. Note that the absolute value of the electric field is its
316 magnitude and the sign represents its direction. In this paper, the direction of electric
317 field produced by DL is taken as positive. As displayed in Figure 3b, in the initial
318 stage of DL propagation (about the first 500 steps), the electric fields increase slowly
319 and there is little difference in electric fields at four corners. As DL gradually
320 approaches the structure, the electric fields at all top corners increase rapidly and the
321 difference in value becomes more and more significant. The electric field at corner
322 NO2 increases at the fastest rate and first reaches the UL initiation threshold. After
323 FUL initiates from corner NO2, the electric fields at remaining corners exhibit diverse
324 changes under the combined influence of FUL and DL. In Figure 3b, the electric field
325 at NO1 first increases followed by decreasing, and then it increases again to the
326 initiation threshold. The electric field at NO4 increases slowly, and the electric field at
327 NO3 even decreased. In fact, changes in electric field are not accidental, but are
328 closely related to the spatiotemporal evolution of the leaders (e.g., Jiang et al., 2015;

Visacro et al., 2017). So what causes the electric fields to exhibit such complex changes?

To answer this question, we divided simulated CG flash event into two stages as marked in Figure 3b, and searched for factors that affect the electric fields at corners in each stage. In the first stage, only DL develops whose location is asymmetric to top corners of the structure. Figure 3c shows the variation of $D_{NO_k}$ versus the DL propagation steps, where $D_{NO_k}$ is defined as the weighted distance between the DL and top corners of the structure, which is given by

$$D_{NO_k} = \sum_{i=1}^{n} g_i \sqrt{(X_i - x_k)^2 + (Y_i - y_k)^2 + (Z_i - z_k)^2} \quad (1)$$

Where $(X_i, Y_i, Z_i)$ is the location of the $i$-th DL channel point in 3-D coordinate system and $(x_k, y_k, z_k)$ is the location of $k$-th top corner ($k$=1,2,3,4). $n$ represents the number of existing DL channel points. $g_i$ is the weight of $i$-th channel point, which is given by $g_i = \frac{1500 - Z_i}{1500 - h}$ for the following reason: In a 3-D simulation domain whose top is 1500m-height, the channel point that appears at a higher altitude ($Z_i$) means it has less impact on the electric fields at the top corners. And $h$ is the structure height (300m in this paper). By qualitatively comparing the electric field change (see Figure 3b) and weighted distance $D_{NO_k}$ (see Figure 3c), a close relationship between the two can be found. That is, a smaller value of $D_{NO_k}$ results in a more rapidly increasing electric field and the greater difference in $D_{NO_k}$ leads to the greater difference in electric fields produced by DL. For this reason, as the electric fields at the top corners increase at unequal rates, the difference in electric fields caused by DL spatial location may already be significant by the time FUL initiates (see Figure 3b).

Once FUL is triggered, the second stage begins. At this stage, the electric fields at remaining corners (NO1, NO3, NO4) is the superposition of the electric field produced by DL, the electric field produced by FUL (defined as $\boldsymbol{E_{FUL}}$) and

353 background electric field which is constant in LAMM. As suggested by Cooray et
354 al.(2010), the presence of a small advantage for the growth of a FUL from one corner
355 may drastically reduce the ability of other corners to launch successful SUL. Thence,
356 it is necessary to analyze the behavior of FUL. Unlike the DL with multi-branches,
357 the length and propagation direction of a single-branch FUL can be clearly obtained in
358 simulation work. The blue line in Figure 3d plots the electric field at corner NO1
359 produced by FUL ($\boldsymbol{E_{FUL}}$) versus the FUL length. As shown in Figure 3d, FUL
360 produces the electric field $\boldsymbol{E_{FUL}}$ whose direction is opposite to that of the electric field
361 caused by DL, and its magnitude increases with FUL length. This result is similar to
362 Zhou et al. (2021). Considering the propagation direction of FUL changes several
363 times, we calculated the distance of each FUL channel point from a corner with the
364 second fastest increasing electric field, which is defined by

365 $$d(j)_{FUL} = \sqrt{\left(X_j - x'\right)^2 + (Y_j - y')^2 + (Z_j - z')^2} \quad (2)$$

366 Where $(X_j, Y_j, Z_j)$ is the location of the $j$-th FUL channel point in 3-D coordinate
367 system and $(x', y', z')$ is the location of the corner with the second fastest increasing
368 electric field (corner NO1 in this case). As $d(j)_{FUL}$ displayed by the red line in
369 Figure 3d, FUL firstly extends 13 steps away from corner NO1, and then propagates
370 11 steps toward corner NO1 before extending away from corner NO1 again. This
371 result is consistent with FUL behaviors presented in Figure 3a, so the factor $d(j)_{FUL}$
372 is used to indirectly show the FUL propagation direction relative to a particular corner.
373 According to the propagation direction of FUL, the variation of electric field $\boldsymbol{E_{FUL}}$ is
374 divided into three phases as shown in Figure 3d. Linear fitting has been performed in
375 each phase to obtain the electric field change rates $\boldsymbol{K_1}$ to $\boldsymbol{K_3}$. The result shows absolute
376 value of $\boldsymbol{K_2}$ is significantly larger than absolute values of $\boldsymbol{K_1}$ and $\boldsymbol{K_3}$, which means the
377 $\boldsymbol{E_{FUL}}$ increases more faster when FUL extends close to the NO1 than that when FUL
378 extends away from it. From the above analysis, it can be inferred that the electric field
379 caused by FUL varies with its length and its propagation direction.

380 In this section, we divided the CG flash event into two stages and found the electric

fields at top corners is related to the weighted distance from DL channel to top corners $D_{NO_k}$, the FUL's length and its propagation direction. In sections 4.2 and 4.3, we will try to explain the reasons for a structure to launch only one UL or MULs based on these factors.

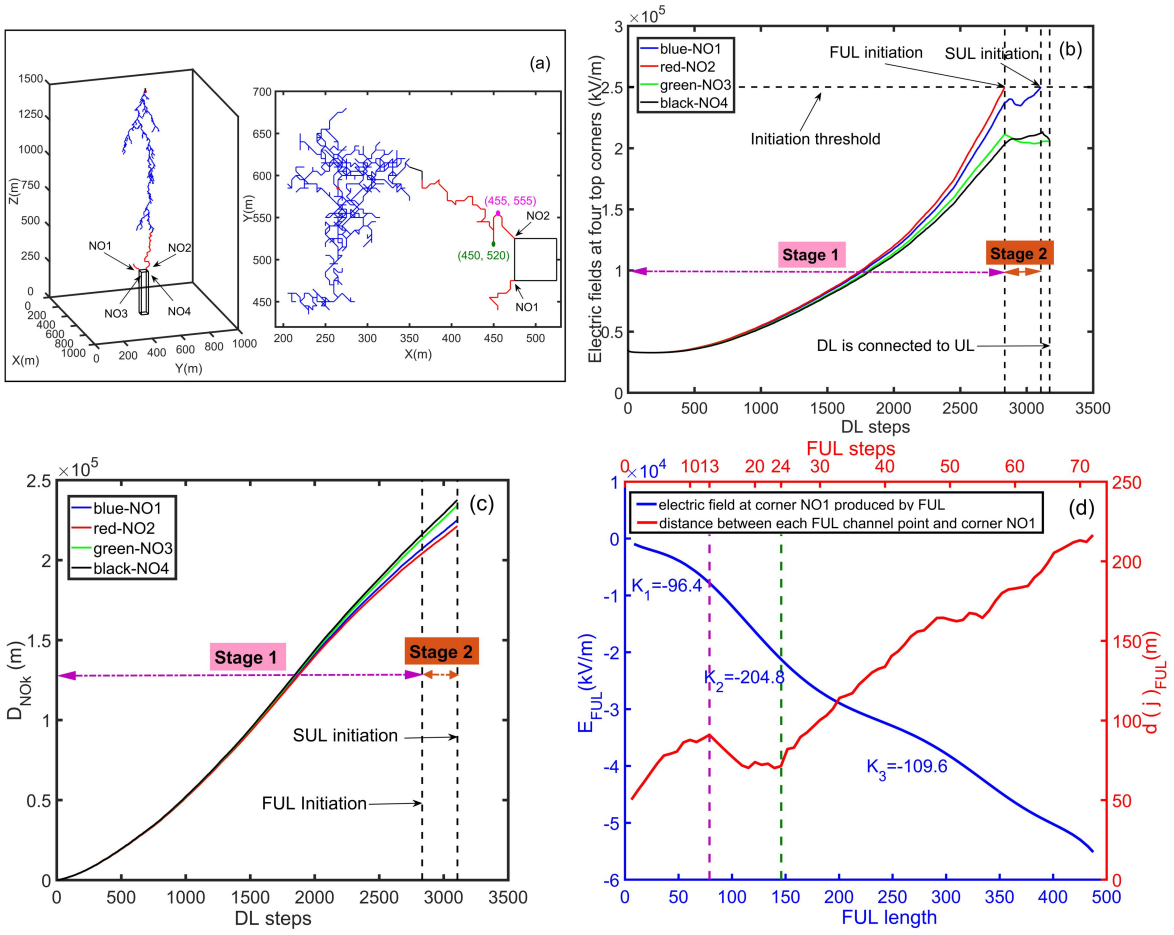


**Figure 3.** A case study: (a) A 3-D CG flash event with two ULs and its 2D projection onto the x-y plane. DL initiates at a location with spatial coordinate (265, 585, 1500), and two turning points in the FUL development process are marked on x-y plane. The details are the same as in Figure 1. (b) The variation of electric field at four top corners with DL propagation, NO1~NO4 represent the four top corners of the structure marked in Figure 3a. (c) The weight distance between DL and four top corners ( $D_{NO_k}$) varies with DL propagation, NO1~NO4 represent the four top corners of the structure as marked in Figure 3a. (d) The blue line denotes the variation of electric field produced by FUL ($\boldsymbol{E_{FUL}}$) at corner NO1 with the length of FUL before SUL occurs. The red line denotes the $d(j)_{FUL}$ at each FUL step before SUL occurs,

which indirectly shows the propagation direction of FUL. The purple and the green dashed lines respectively represent two moments at which the propagation direction of FUL significantly changes, corresponding to the two turning points in Figure 3a. The variation of $\boldsymbol{E_{FUL}}$ is divided into three phases according to the propagation direction of FUL. And $\boldsymbol{K_1}$ ***to*** $\boldsymbol{K_3}$ are the electric field change rates in each phase. For definition details of $D_{NO_k}$ and $d(j)_{FUL}$ see formulas (1) and (2).

4.2 The first stage: only DL propagates

Since the tortuous nature of DL and spatial asymmetry of DL relative to the structure causing different places of a structure almost never experience the same electric field at the same time, the electric fields at top corners increase at unequal rates. Considering that the amount of DL channel points varies from flash to flash, $\overline{D}_{dif}$ is defined as the difference in the average weighted distance between DL to the corners with the fastest and the second fastest increasing electric field, which is given by:

$$\overline{D}_{dif} = \frac{1}{n}\left|D_{NO_k(1)} - D_{NO_k(2)}\right| \tag{3}$$

Where $D_{NO_k(1)}$ and $D_{NO_k(2)}$, calculated by equation (1), corresponding the electric fields at the fastest and second fastest increasing rates in the same CG flash event, respectively. $n$ is the number of DL channel points in a CG flash simulation. Figure 4 depicts the distribution of $\overline{D}_{dif}$ in the four scenarios mentioned in section 3. Obviously, the $\overline{D}_{dif}$ in the flash events with MULs (Scenarios A and B) is smaller than $\overline{D}_{dif}$ in the flash events with only one UL (Scenarios C and D), and this difference is especially noticeable in scenarios A and D. From this, it can be inferred that if the $\overline{D}_{dif}$ is small, the structure has a higher probability of launching MULs than occurring one UL. When $\overline{D}_{dif}$ is less than 0.8m, we consider after FUL initiates, the SUL will appear on the structure sooner or later (a 3.45% error). If $\overline{D}_{dif}$ is too large, that is, $\overline{D}_{dif}$ exceeds a critical value of 4m in a CG flash simulation, it is

considered that only one UL can initiate from a 300-m-tall structure (a 4.89% error).

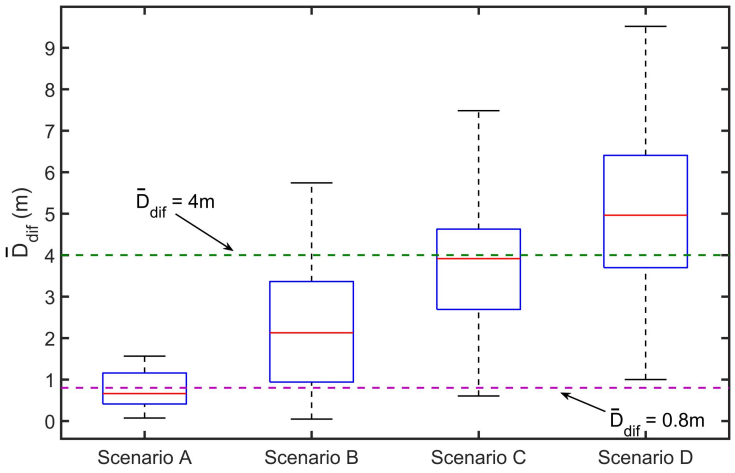


**Figure 4.** The difference in the average weighted distance between DL to the corners with the fastest and second fastest increasing electric field ($\overline{D}_{dif}$) in four scenarios. The purple and green lines represent the critical values of $\overline{D}_{dif}$ of 0.8m and 4m, respectively. For definition details see formula (3).

Two cases (see Figure 5) where $\overline{D}_{dif} \leq 0.8m$ and $\overline{D}_{dif} \geq 4m$ are taken as examples to explain one of the situations where one UL and MULs occur. In Figure 5a, a $\overline{D}_{dif}$ value of 0.41m indicates that there is little difference in the increasing rates of electric fields at corner NO1 and corner NO2. After FUL initiates from corner NO1, it only needs DL to continue to produce a small positive electric field at corner NO2 to meet the UL initiation threshold. This is easy for DL that is approaching, so the SUL will appear sooner or later. In Figure 5b, a $\overline{D}_{dif}$ value of 5.91m means the great difference in the positive electric field changes at corners NO3 and NO4 produced by DL. Therefore, after FUL appears on corner NO3, it needs DL to continuously produce a quite large positive electric field at corner NO4. What is even more unfavorable for the SUL inception is that the reverse electric field is continuing to intensify with the extension of FUL. Therefore, it is very difficult for the electric field at corner NO4 to reach the UL initiation threshold, resulting in only one UL appearing. Note that the critical values of 0.8-m and 4-m are calculated under certain conditions.

If the simulation conditions are changed, critical values should be updated, but we believe that the distance difference $\overline{D}_{dif}$ is always one of the important factors affecting the initiation of upward leaders during the flash attachment process.

As mentioned above, when $\overline{D}_{dif} \leq 0.8m$ or $\overline{D}_{dif} \geq 4m$, some CG flash events with MULs (some cases of scenarios A and B) or one UL (some cases of scenarios C and D) can be identified using the factor $\overline{D}_{dif}$. But when $0.8\text{m} < \overline{D}_{dif} < 4m$, only the factor $\overline{D}_{dif}$ is not enough because four scenarios may occur as revealed in Figure 4. Actually, even though the effect of DL ($\overline{D}_{dif}$) is similar for some corners, electric field changes at these corners may exhibit the opposite trend in the second stage. For example (see Figure 5a), the electric field at corners NO3 and NO4 increases at almost the same rate in the first stage, while in the second stage, the electric field at corners NO3 increases (green line) but the electric field at corner NO4 decreases (black line). A similar result is also shown by corners NO1 and NO3 in Figure 7c. Such cases indicate the same FUL may have a quite different effect on electric fields at different corners in the second stage. Therefore, it is necessary to carry out research on leader behaviors in the second stage.

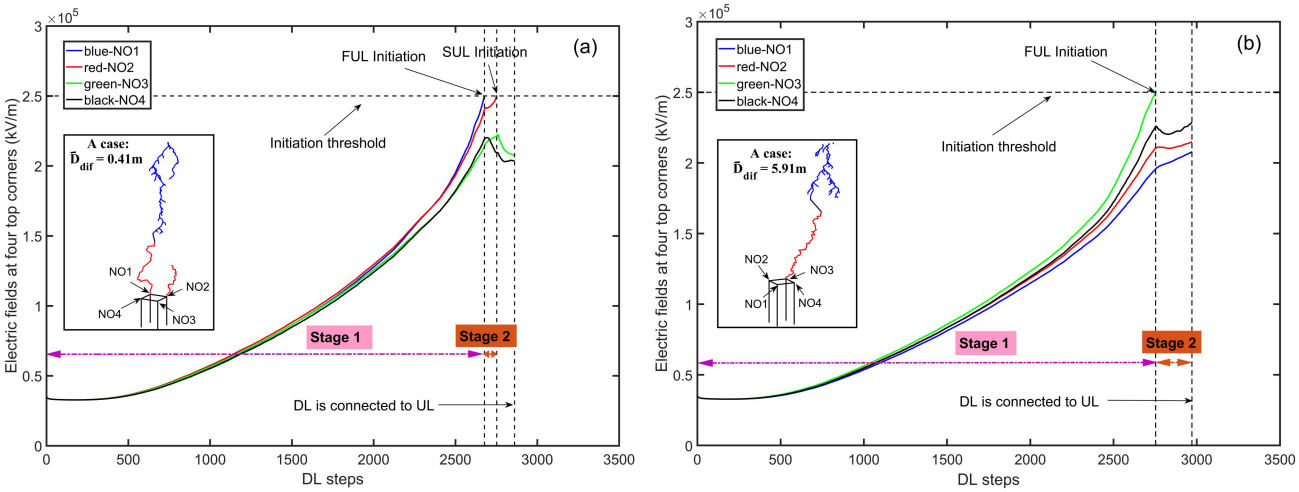


**Figure 5.** Electric field change at four top corners with DL extension in two examples of the flash events with one and two ULs determined by only factor $\overline{D}_{dif}$. (a) A case

where $\overline{D}_{dif} = 0.41m$ and MULs occur. (b) An case where $\overline{D}_{dif} = 5.91m$ and only a single UL occurs. A portion of the 3-D plots corresponding to the electric field changes are shown in the black boxes on the left, respectively. The legends of 3-D plots are the same as that of Figure 1 and the viewing angle is adjusted to better show the simulation results.

### 4.3 The second stage: FUL and DL coexist

Once the structure launches the FUL, the second stage begins, in which FUL and DL coexist. Two factors $e_{DL}$ and $e_{FUL}$ defined based on the analysis in section 4.1 are used to characterize the impact of DL and FUL, respectively, as follows:

$$e_{DL} = \left(\frac{1}{4n}\sum_{k=1}^{4} D_{NO_k}\right)^{-1} \tag{4}$$

Where $D_{NO_k}$ of four top corners are given by equation (1) and $n$ is the number of existing DL channel points. The formula $\frac{1}{4n}\sum_{k=1}^{4} D_{NO_k}$ represents the weighted distance from the overall lightning channel to the structure, which is inversely correlated with the electric fields at top corners (see section 4.1). Hence, the above formula is transformed to its inverse proportional function as shown in equation (4). Considering that the electric field produced by FUL is affected by its length and direction, $e_{FUL}$ is given by:

$$e_{FUL} = \sum_{j=1}^{m} \frac{l_j}{d(j)_{FUL}} \tag{5}$$

Where $l_j$ is the length of new FUL channel segment at the $j$-th step and $m$ is the number of current FUL channel points. $d(j)_{FUL}$ given by equation (2) is the distance from FUL to the corner with second fastest increasing electric field. The larger the value of $e_{DL}$ or $e_{FUL}$, the greater the impact of DL or FUL on electric fields at top corners. It is clear from Figure 6 that the $e_{DL}$ and $e_{FUL}$ in scenarios A and D are significant differences from that in other scenarios. $e_{DL}$ is the largest in scenario A, the smallest in scenario D, and the opposite is true for $e_{FUL}$.

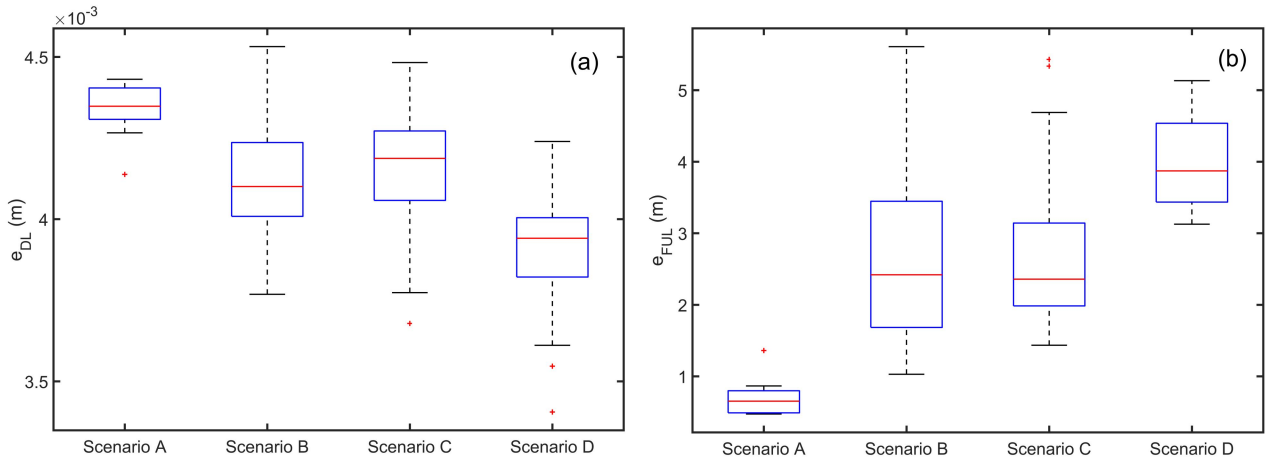


**Figure 6.** The distribution of two factors in four scenarios. (a) $e_{DL}$, which represents the effect of DL on the electric fields at the top corners. (b) $e_{FUL}$, which represents the effect of FUL on the electric field at the corner with the second fastest increasing rate before FUL occurs. For definition details see formulas (4) and (5).

Two examples as shown in Figures 7a and 7d are taken to explain scenario A and scenario D. In Figure 7a, a very small $\overline{D}_{dif}$ (see Figure 4) leads to the electric fields at corner NO1 and corner NO2 increase at almost the same rate in the first stage. In the second stage, the DL which is close to a structure (see Figure 6a) produces a great positive electric field, causing the electric field at corner NO1 to exceed the UL initiation threshold after FUL extends only a few steps (Scenario A). During this period, the effect of FUL is weak (see Figure 6b). While in Figure 7d, DL is far away from the structure, the impact of DL on electric fields at top corners is weak (see Figure 6a). Meanwhile, since the UL has to propagate a large distance towards the distant DL in order to connect to it, a long-length FUL produces a great reverse electric field (see Figure 6b). Thence, after FUL occurs on corner NO4, the electric fields at other corners decrease and have no chance to reach UL initiation threshold as shown in Figure 7d, resulting in a single long-length UL occurring on the structure (Scenario D).

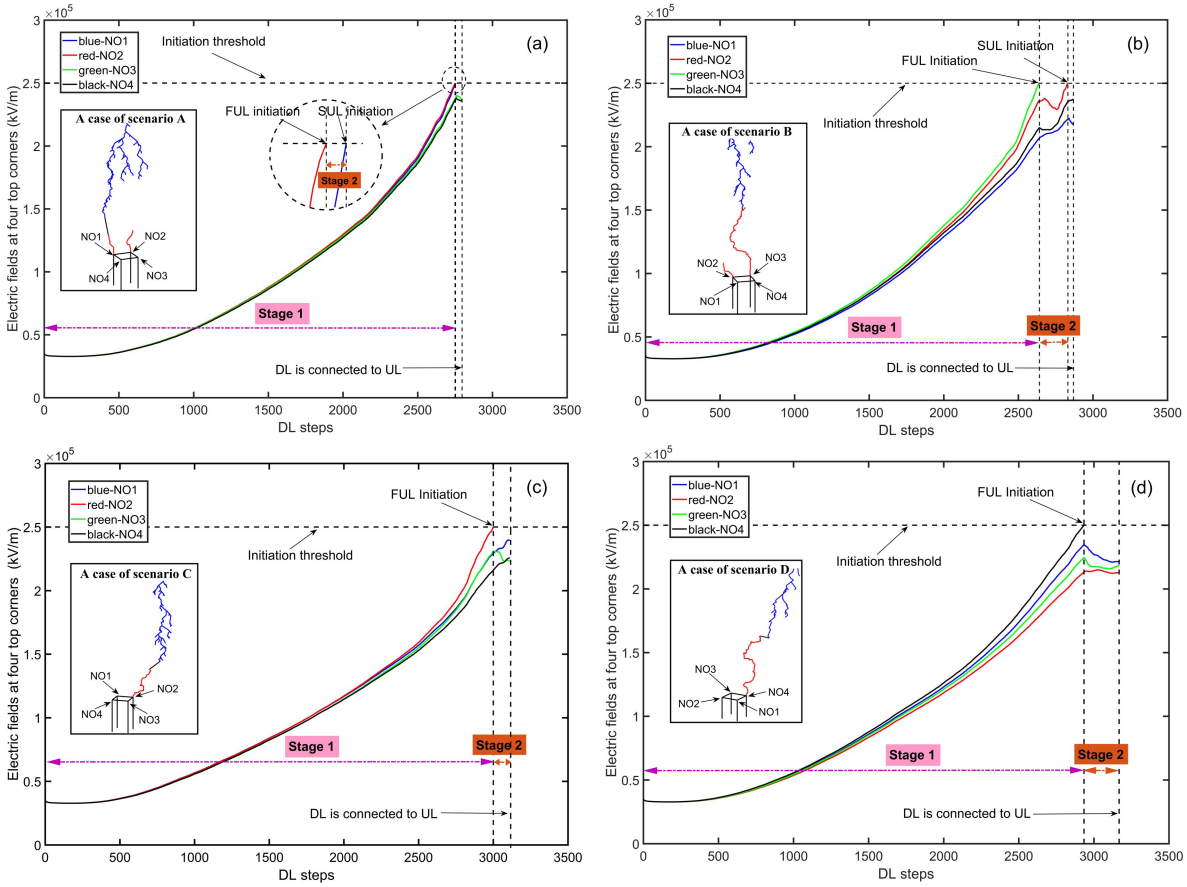


498 **Figure 7.** Variation of electric fields at the top corners with DL extension in four
499 examples corresponding to the four scenarios. (a) A case of scenario A. (b) A case of
500 scenario B. (c) A case of scenario C. (d) A case of scenario D. Legends are the same
501 as those of Figure 5.

502 However, it is still hard to explain why MULs occur in scenario B but only a single
503 UL occurs in scenario C, because the factors of $e_{DL}$ and $e_{FUL}$ are similar (see Figure
504 6), and the difference in $\overline{D}_{dif}$ (see Figure 4) is not sufficient to identify the two
505 scenarios well. Therefore, we further analyzed the electric field changes at the top
506 corners in scenarios B and C in the second stage. It can be found that although the
507 electric field at corners without FUL may increase or decrease in the first few steps of
508 DL propagation, the electric fields at some corners in both scenarios eventually tend
509 to increase (see the examples in Figures 7b and 7c). We suggest one possible reason
510 as follows: when FUL has developed only a few steps, neither DL nor UL has a
511 commanding influence on the electric field changes at top corners in scenarios B and

C. While, since the average propagation speed of DL is faster than that of UL's (Saba et al., 2017; Yokoyama et al., 1990), DL will gradually gain dominance as it continues to extend downward, causing the electric fields at some top corners to increase. Hence, in a sense, the SUL can be triggered if there is sufficient time for electric field to increase in scenarios B and C. Unfortunately, time is limited because the occurrence of final jump breaks the increasing trend of electric field. Thus, we believe the time interval from FUL initiation to final jump, which is represented by $T_{step}$, is also a critical factor. Since there is no realistic time in LAMM, the $T_{step}$ is defined by the number of steps the FUL propagates from its inception to final jump. As shown in Figure 8, the time interval in scenario B is significantly longer than that in scenario C. This indicates the final jump occurs more slowly in scenario B, which allows the electric field to have enough time to increase to UL inception threshold, thereby initiating SUL. While in scenario C, the positive leader is connected to the negative leader soon after FUL occurs. Thence, even if the electric field has a trend of increasing, it is too late to reach the initiation threshold, causing only a short-length UL occurs on the structure.

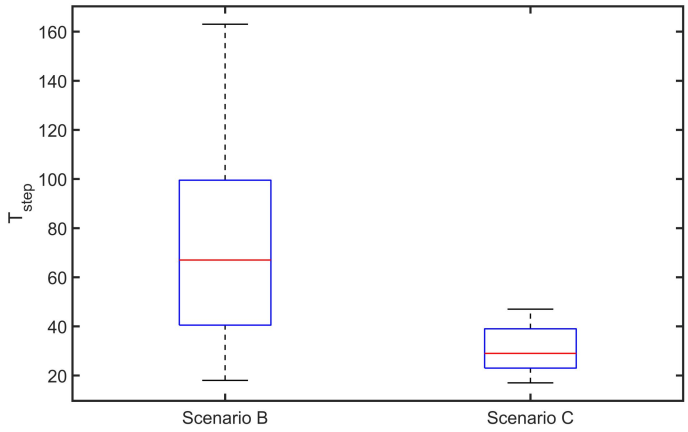


**Figure 8.** The distribution of $T_{step}$ in scenarios B and C. $T_{step}$ indirectly represents the time interval from FUL initiation to final jump.

## 5 Conclusions

Focusing more on the behavior of downward and upward leaders, this paper discussed

whether the SUL is initiated after FUL appears on a single structure. Here, a 3-D fine-resolution lightning attachment model with MULs (LAMM) is established based on the existing stochastic discharge parameterization scheme for research. In order to simulate the CG flash in a larger 3-D domain without sacrificing resolution as much as possible, the GPU parallel computing technology has been used to speed up iterative tasks. The model can reproduce one or more ULs initiating from one or more structures with any size. And the successful simulation of diverse lightning structures and tortuous development of leaders, which resemble actual electrical discharges, lend credence to the LAMM has certain advantages in researching the influence of leader spatial behaviors on the lightning attachment process.

We used the LAMM with grid spacing of 5m to simulate 300 CG flash events in a domain of 1000m × 1000m × 1500m. The simulation results of lightning terminating on a 300m-height structure were divided into the following four scenarios: A, FUL and SUL initiate almost simultaneously; B, SUL is triggered much later than FUL; C, a single UL with short length occurs on the structure; D, the structure launches only one long-length UL. Our qualitative analysis in each scenario suggests the significant influence of the spatial behavior of the positive and negative leaders on the ambient electric field and further effect the inception of SUL. From this, each simulated discharge process was divided into two stages according to whether the FUL initiated and the following four relevant factors were proposed. $\overline{D}_{dif}$ is the difference in the average weighted distance between DL to the top corners with the fastest and the second fastest increasing electric field in the first stage. In the second stage, we proposed three other factors. $e_{DL}$ reflects the distance between the lightning overall channel to the structure and $e_{FUL}$ is defined by the length and propagation of FUL. They are used to characterize the impact of DL and UL, respectively. In addition, $T_{step}$ represents the time interval from FUL initiation to final jump. With these four factors, we explained why the above four scenarios happen. The details are as follows.

559 The $\overline{D}_{dif}$ in the flash events with MULs (Scenarios A and B) is smaller than $\overline{D}_{dif}$ in
560 the flash events with only one UL (Scenarios C and D). And this factor alone can
561 distinguish between some cases with MULs and some cases with one UL. If $\overline{D}_{dif} \leq$
562 $0.8m$, SUL can occur on the structure soon or later (some cases of scenarios A and B),
563 because it only needs a small positive electric field produced by DL after FUL occurs.
564 If $\overline{D}_{dif} \geq 4m$, the structure can launch only one UL (some cases of scenarios C and
565 D), because the UL initiation threshold can not be reached again before the final jump
566 takes place under the influence of FUL. Note that even if the critical values should be
567 updated according to different simulation conditions, $\overline{D}_{dif}$ is always one of the
568 important factors affecting SUL inception. Since the four scenarios may occur when
569 $0.8\text{m} < \overline{D}_{dif} < 4$, we added three more factors to discuss the second stage. After
570 FUL is triggered, if there is a large $e_{DL}$ value and a small $e_{FUL}$ value, SUL can
571 initiate after FUL extend a few steps (Scenario A). While a small value of $e_{DL}$ and a
572 large value of $e_{FUL}$ result in only a long-length UL appearing on the structure,
573 because DL only produce a small positive electric field at top corners and there is a
574 great reverse electric field produced by FUL (Scenario D). But in scenarios B and C,
575 the factors of $e_{DL}$ and $e_{FUL}$ are similar, and the different in $\overline{D}_{dif}$ is not sufficient to
576 identify the two scenarios well. Due to the electric fields at some top corners can
577 finally show an increasing trend as DL approaches in both scenarios B and C, we
578 believe the $T_{step}$ is critical. If the final jump occurs slowly (a large $T_{step}$), the electric
579 fields at corners have enough time to increase to the UL initiation threshold, thereby
580 the SUL can appear (Scenario B). If final jump occurs too fast (a small $T_{step}$), it is too
581 late to generate SUL resulting in only a short-length UL initiating (Scenario C).

582 To a certain extent, this study explains the reasons for the emergence of MULs, which
583 is conducive to deepen the understanding of the CG lightning process. However, the
584 inception of MULs is also caused by many other factors. Limited by the

parameterization scheme, we cannot analyze micro discharge process and the charge structure in thunderstorm clouds. And the effect of other factors such as structure-height and lightning intensity are not discussed in this paper, which is a target for our future work.

**Acknowledgments**

- The work was supported by the National Key Research and Development Program of China (2017YFC1501504), the National Natural Science Foundation of China (Grant No. 41875003, 41805002) and the Open Research Program of the State Key Laboratory of Severe Weather (Grant No. 2019LASW-A03). The authors would like to express their sincerely thanks to all the people giving an assistance.

**References**

Aleksandrov, N. L., Bazelyan, E. M., Carpenter, Jr. R. B., Drabkin, M. M., & Raizer, Y. P. (2001), The effect of coronae on leader initiation and development under thunderstorm conditions and in long air gaps. *Journal of Physics D: Applied Physics*, *34*(22), 3256-3266. doi:10.1088/0022-3727/34/22/309

Arevalo, L., & Cooray,V. (2009), Influence of multiple upward connecting leaders initiated from the same structure on the lightning attachment process. *X International Symposium on Lightning Protection*. Center for Science and Technology of the Non-Aligned and other Developing Countries, Curitiba, Brazil.

Bazelyan, E. M., Raizer, Y. P. , Aleksandrov, N. L., & D'Alessandro, F. (2009), Corona processes and lightning attachment: The effect of wind during thunderstorms. *Atmospheric Research*, *94*(3), 436 – 447. doi:10.1016/j.atmosres.2009.07.002

Becerra, M., & Cooray, V. (2006), A simplified physical model to determine the lightning upward connecting leader inception. IEEE Transactions on Power Delivery, 21(2), 897 – 908. doi:10.1109/TPWRD.2005.859290

Becerra, M., & Cooray, V. (2008), On the velocity of positive connecting leaders associated with negative downward lightning leaders. *Geophysical Research Letters*,

613 *35*, L02801. doi:10.1029/2007GL032506
614 Bermudez, J. L., Rachidi, F., Janischewskyj, W., Hussein, A. M., Rubinstein, M.,
615 Nucci, C. A., et al. (2001), On the enhancement of radiated electric and magnetic
616 fields associated with lightning return strokes to tall structures. *IEEE International*
617 *Symposium on Electromagnetic Compatibility*, *2*, 1005–1008.
618 doi:10.1109/ISEMC.2001.950535
619 Biagi, C. J., Jordan, D. M., Uman, M. A., Hill, J. D., Beasley, W. H., & Howard, J.
620 (2009), High speed video observations of rocket-and-wire initiated lightning.
621 Geophysical Research Letters, 36, L15801. doi:10.1029/2009GL038525
622 Biagi, C. J., Uman, M. A., Gopalakrishnan, J., Hill, J. D., Rakov, V. A., Ngin, T. &
623 Jordan D. M. (2011), Determination of the electric field intensity and space charge
624 density versus height prior to triggered lightning. Journal of Geophysical Research,
625 116, D15201. doi:10.1029/2011JD015710
626 Biagi, C. J., Uman, M. A., Hill, J. D., & Jordan, D. M. (2014), Negative leader step
627 mechanisms observed in altitude triggered lightning. *Journal of Geophysical*
628 *Research: Atmospheres*, *119*, 8160–8168. doi:10.1002/2013JD020281
629 Chauzy, S., Medale, J. C., Prieur, S., & Soula, S. (1991), Multilevel measurement of
630 the electric field underneath a thundercloud. A new system and the associated data
631 processing. Journal of Geophysical Research, 96 (D12), 22319–22326.
632 doi:10.1029/91jd02031
633 Chernov, E. N., Lupeiko, A. V. & Petrov, N. I. (1991), Investigation of spark
634 discharge in long air gaps using Pockel's device. *Proceeding 7th International*
635 *Symposium on High Voltage Engineering*, Dresden, Germany.
636 Cooray, V., Fernando, M., Arevalo, L., & Becerra, M. (2010), Interaction of multiple
637 connecting leaders issued from a grounded structure simulated using a self consistent
638 leader inception andropagation model (slim). *Proceedingsof the 30th International*
639 *Conference on Lightning Protection*, Cagliari, Italy. doi:101109/ICLP.2010.7845803
640 Dellera, L., & Garbagnati, E. (1990), Lightning stroke simulation by means of the
641 Leader Progression Model: I. Description of the model and evaluation of exposure of
642 free-standing structures. *IEEE Transactions on Power Delivery*, *5*(4), 2009–2022.

643 doi:10.1109/61.103696
644 Dul'zon, A. A., Lopatin, V., Noskov, M., & Pleshkov, O. (1999), Modeling the
645 development of the stepped leader of a lightning discharge. *Technical Physics*, *44* (4),
646 394–398. doi:10.1134/1.1259308
647 Gao, Y., Lu, W., Ma, Y., Chen, L., Zhang, Y., & Yan, X. (2014), Three-dimensional
648 propagation characteristics of the upward connecting leaders in six negative
649 tall-object flashes in Guangzhou. *Atmospheric Research*, *149*, 193–203.
650 doi:10.1016/j.atmosres.2014.06.008
651 Gurevich, A. V., & Zybin, K. P. (2001), Runaway breakdown and electric discharges
652 in thunderstorms. Physics Uspekhi, 44 (11), 1119. doi:10.1029/2009JA014818
653 Hill, J. D., Uman, M. A., & Jordan, D. M. (2011), High-speed video observations of a
654 lightning stepped leader. *Journal of Geophysical Research*, *116*, D16117.
655 doi:10.1029/2011JD015818
656 Iudin, D. I., Rakov, V. A., Mareev, E. A., Iudin, F. D., Syssoev, A. A., & Davydenko, S.
657 S. (2017), Advanced numerical model of lightning development: Application to
658 studying the role of LPCR in determining lightning type. *Journal of Geophysical*
659 *Research: Atmospheres*, *22*(12), 6416–6430. doi:10.1002/2016JD026261
660 Jiang, R., Lyu, W., Wu, B., Qi, Q., Ma, Y., Su, Z., et al. (2020), Simulation of
661 cloud-to-ground lightning strikes to structures based on an improved stochastic
662 lightning model. *Journal of Atmospheric and Solar-Terrestrial Physics*, *203*, 105274.
663 doi:10.1016/j.jastp.2020.105274
664 Jiang, R., Qie, X., Wang, Z., Zhang, H., Lu, G., Sun, Z., et al. (2015), Characteristics
665 of lightning leader propagation and ground attachment. *Journal of Geophysical*
666 *Research: Atmospheres*, *120*, 11988–12002. doi:10.1002/2015JD023519
667 Krider, E., & Ladd, C. J. W. (1975), Upward streamers in lightning discharges to
668 mountainous terrain. *Weather*, *30* (3), 77–81.doi:10.1002/j.1477-8696.1975.tb05282.x
669 Lu, W., Chen, L., Ma, Y., Rakov, V. A., Gao, Y., Zhang, Y., et al. (2013), Lightning
670 attachment process involving connection of the downward negative leader to the
671 lateral surface of the upward connecting leader. Geophysical Research Letters, 40,
672 5531–5535. doi:10.1002/2013GL058060

673 Lu, W., Chen, L., Zhang, Y., Ma, Y., Gao, Y., Yin, Q., et al. (2012), Characteristics of
674 unconnected upward leaders initiated from tall structures observed in Guangzhou.
675 Journal of Geophysical Research, 117, D19211. doi:10.1029/2012JD018035
676 Lu, W., Qi, Q., Ma, Y., Chen, L., Yan, X., Rakov, V., et al. (2016), Two basic leader
677 connection scenarios observed in negative lightning attachment process. *High Voltage,*
678 *1*(1): 11-17. doi: 10.1049/hve.2016.0002.
679 Mansell, E. R., MacGorman, D. R., Ziegler, C. L., & Straka, J. M. (2002), Simulated
680 three-dimensional branched lightning in a numerical thunderstorm model. *Journal of*
681 *Geophysical Research*, *107*(D9), 1–2. doi:10.1029/2000JD000244
682 Mazur, V., Ruhnke, L. H., Bondiou-Clergerie, A., & Lalande, P. (2000), Computer
683 simulation of a downward negative stepped leader and its interaction with a ground
684 structure. *Journal of Geophysical Research: Atmospheres*, *105* (D17), 22361–22369.
685 doi:10.1029/2000JD900278
686 Motoyama, H., Janischewskyj, W., Hussein, A. M., Rusan, R., Chisholm, W. A., &
687 Chang, J. S. (1996), Electromagnetic field radiation model for lightning strokes to tall
688 structures. *IEEE Transactions on Power Delivery*, *11*(3), 1624–1632.
689 doi:10.1109/61.517526
690 Petrov, N. I., Avanskii, V. R., & Bombenkova, N. V. (1994), Measurement of the
691 electric field in the streamer zone and in the sheath of the channel of leader discharge.
692 Technical Physics, 39, 546–551.
693 Petrov, N. I., & D'Alessandro, F. (2002), Theoretical analysis of the processes
694 involved in lightning attachment to earthed structures. Journal of Physics D: Applied
695 Physics, 35(14), 1788–1795. doi:10.1088/0022-3727/35/14/321
696 Petrov, N. I., Petrova, G., & D'Alessandro, F. (2003), Quantification of the probability
697 of lightning strikes to structures using a fractal approach. *IEEE Transactions on*
698 *Dielectrics and Electrical Insulation*, 10 (4), 641–654.
699 doi:10.1109/TDEI.2003.1219649
700 Qi, Q., Lu, W., Ma, Y., Chen, L., Zhang, Y., & Rakov, V. A. (2016), High-speed video
701 observations of the fine structure of a natural negative stepped leader at close distance.
702 Atmospheric Research, 178-179, 260–267. doi:10.1016/j.atmosres.2016.03.027

703 Qi, Q., Lyu, W., Ma, Y., Wu, B., Chen, L., Jiang, R., et al. (2019), High-speed video
704 observations of natural lightning attachment process with framing rates up to half a
705 million frames per second. *Geophysical Research Letters*, *46*, 12580–12587.
706 doi:10.1029/2019GL085072
707 Qi, Q., Lyu, W., Wang, D., Wu, B., Ma, Y., Chen, L., et al. (2021), Two-dimensional
708 striking distance of lightning flashes to a cluster of tall buildings in Guangzhou.
709 Journal of Geophysical Research: Atmospheres, 126(22). doi:10.1029/2021JD034613
710 Rakov, V., &Uman, M. (2003), Lightning: Physics and Effects, Cambridge University
711 Press, New York.
712 Riousset, J. A., Pasko, V. P., Krehbiel, P. R., Thomas, R. J., & Rison, W. (2007), Three
713 dimensional fractal modeling of intracloud lightning discharge in a New Mexico
714 thunderstorm and comparison with lightning mapping observations. *Journal of*
715 *Geophysical Research*, *112*, D15203. doi:10.1029/2006JD007621
716 Saba, M. M. F., Paiva, A. R., Schumann, C., Ferro, M. A. S., Naccarato, K. P., Silva,J.
717 C. O., et al. (2017), Lightning attachment process to common buildings. Geophysical
718 Research Letters, *44*, 4368–4375. doi:10.1002/2017GL072796
719 Stolzenburg, M., Marshall, T. C., Karunarathne, S., Karunarathna, N. & Orville, R. E.
720 (2015), Transient luminosity along negative stepped leaders in lightning. *Journal of*
721 *Geophysical Research: Atmospheres*, 120, 3408–3435. doi:10.1002/2014JD022933
722 Syssoev, A. A., Iudin, D. I., Bulatov, A. A., & Rakov, V. A. (2020), Numerical
723 simulation of stepping and branching processes in negative lightning leaders. *Journal*
724 *of Geophysical Research: Atmospheres*, *125*(7). doi:10.1029/2019JD031360
725 Tan, Y., Guo, X., Zhu, J., Shi, Z. & Zhang, D. (2014a), Influence on simulation
726 accuracy of atmospheric electric field around a building by space resolution.
727 Atmospheric Research, 138, 301–307. doi:10.1016/j.atmosres.2013.11.023
728 Tan, Y., Tao, S., Liang, Z., & Zhu, B. (2014b), Numerical study on relationship
729 between lightning types and distribution of space charge and electric potential.
730 Journal of Geophysical Research: Atmospheres, 119, 1003–1014.
731 doi:10.1002/2013JD019983
732 Tan, Y., Tao, S., & Zhu, B. (2006), Fine-resolution simulation of the channel

733 structures and propagation features of intracloud lightning. *Geophysical Research*
734 *Letters*, *33*(9), L09809. doi:10.1029/2005GL025523
735 Tao, S., Tan, Y., Zhu, B., Ma, M., & Lu, W. (2009), Fine-resolution simulation of
736 cloud-to-ground lightning and thundercloud charge transfer. *Atmospheric Research*,
737 *91* (2-4), 360–370. doi:10.1016/j.atmosres.2008.05.012
738 Tran, M. D., Rakov, V. A., & Mallick, S. (2014), A negative cloud-to-ground flash
739 showing a number of new and rarely observed features. Geophysical Research Letters,
740 41, 6523–6529. doi:10.1002/2014GL061169
741 Tran, M. D., & Rakov, V. A. (2017), A study of the ground-attachment process in
742 natural lightning with emphasis on its breakthrough phase. *Scientific Reports*, *7*,
743 15761. doi:10.1038/s41598-017-14842-7
744 Visacro, S., Guimaraes, M., & Murta Vale, M. H. (2017), Features of upward positive
745 leaders initiated from towers in natural cloud-to-ground lightning based on
746 simultaneous high-speed videos, measured currents, and electric fields. *Journal of*
747 *Geophysical Research: Atmospheres*, *122*, 12786 – 12800.
748 doi:10.1002/2017JD027016
749 Wang H., Guo, F., Zhao, T., Qin, M., & Zhang, L. (2016), A numerical study of the
750 positive cloud-to-ground flash from the forward flank of normal polarity thunderstorm.
751 Atmospheric Research, 169, 183-190. doi:10.1016/j.atmosres.2015.10.011
752 Wang, X., Zhao, X., Hao, Y., Cai, H., Liu, G., Liao, M., & Qu, L. (2019), High-speed
753 video observations of branching behaviors in downward stepped leaders and upward
754 connecting leaders in negative natural lightning. *Journal of Atmospheric and*
755 *Solar-Terrestrial Physics*, *183*, 61 – 66. doi:10.1016/j.jastp.2018.12.010
756 Warner, T. A. (2010), Upward leader development from tall towers in response to
757 downward stepped leaders. paper presented at 2010 30th International Conference on
758 Lightning Protection, IEEE, Cagliari, Italy. doi:10.1109/ICLP.2010.7845809
759 Xu, D., Tan, Y., Zheng, T., Lin, H., Shi, Z., Lei, Y., et al. (2021), Numerical simulation
760 on the effects of the horizontal charge distribution on lightning types and behaviors.
761 *Journal of Geophysical Research: Atmospheres*, *126*(18). doi:10.1029/2020JD034375
762 Yokoyama, S., Miyake, K., Suzuki, T., & Kanao, S. (1990), Winter lightning on Japan

763 Sea coast-development of measuring system on progressing feature of lightning
764 discharge. *IEEE Transactions on Power Delivery*, *5*(3), 1418–1425.
765 doi:10.1109/61.57984
766 Zhou, M., Ding, W. H., Wang, J. G., Cai, L., Li, Q. X., & Fan, Y. D. (2021), Effects of
767 long upward connecting leader channel on electromagnetic fields for lightning
768 striking to tall towers. *IEEE Transactions on Electromagnetic Compatibility*,
769 *63*(5):1461–1470. doi:10.1109/temc.2021.3068720